

Decay studies of neutron-deficient nuclei near the $Z = 64$ subshell: ^{141}Dy , ^{141}Tb , $^{141}\text{Gd}^g + m$, and $^{141}\text{Eu}^m$

J. Gilat,* J. M. Nitschke, P. A. Wilmarth, and R. B. Firestone

Nuclear Science Division, Lawrence Berkeley Laboratory, 1 Cyclotron Road, Berkeley, California 94720

(Received 25 July 1989)

The β/γ and delayed proton decays of mass separated $A = 141$ isotopes with $Z = 63-66$ were investigated with an on-line mass separator. Branching ratios have been redetermined for the total β decay of the 2.7(3) s, $\frac{11}{2}^-$ isomer $^{141}\text{Eu}^m$ at 96.5 keV ($13 \pm 2\%$), and for the direct β feeding of the 1.58 keV $\frac{3}{2}^+$ level of ^{141}Sm in the decay of 40-s $^{141}\text{Eu}^g$ [73(5)%]. Detailed decay schemes have been constructed for the decays of the $\frac{11}{2}^-$ isomer $^{141}\text{Gd}^m$ [11(2)% isomeric transition] and the $\frac{1}{2}^+$ ground state, $^{141}\text{Gd}^g$. Half-lives of 24.5(5) s and 14(4) s, respectively, have been determined for these isomers. A delayed proton branch of 0.03(1)% was identified in the decay of $^{141}\text{Gd}^g$. A detailed decay scheme was also constructed for 3.5(2)-s ^{141}Tb and a $J^\pi = \frac{5}{2}^-$ was assigned to its ground state, at variance with the systematics of heavier, odd-mass Tb isotopes. All γ -ray assignments to the various isotopes are based on $x\gamma$ and $\gamma\gamma$ coincidences and on half-life measurements. A 0.9(2)-s half-life for ^{141}Dy was determined from its delayed proton decay. All spin assignments proposed in this paper are discussed in terms of Nilsson level diagrams and nuclear shapes.

I. INTRODUCTION

The shapes of nuclei with $50 \leq Z$, $N \leq 82$, and their effect on the structure and spectroscopic properties of these nuclei have been the subject of considerable recent interest. Ragnarsson *et al.*^{1,2} and Leander and Möller³ have predicted relatively stable prolate ground-state shapes for $N < 76$. Meyer-Ter-Vehn⁴ proposed a quasi-particle coupled to a triaxial core configuration to interpret the spectra of $N = 74-78$ odd- A nuclei in the $A = 135$ region. More recently, Cizewski and Gülmez⁵ concluded that the $Z = 64$ shell gap disappears below $N = 78$, with the resulting onset of prolate or triaxial deformation. Rather extensive calculations based on the Strutinsky method and a Woods-Saxon potential for $50 < Z$, $N < 82$, reported by Kern *et al.*,⁶ also predict a region of triaxial deformation around $N = 76-78$. Self-consistent calculations by Redon *et al.*⁷ of the potential-energy surface for triaxial quadrupole deformations in neutron-deficient samarium isotopes again predict triaxial deformations at $N = 76$.

Experimental data lag appreciably behind the theoretical predictions, with an emphasis on in-beam studies of rotational bands more relevant to high-spin spectrometry than to ground-state shapes and deformations of the investigated nuclides.⁸⁻¹³ The growing body of spectroscopic data [E_{4+}/E_{2+} ratios, $B(E2)$ values, moments of inertia, etc.] yields experimental support to theoretical predictions regarding the shapes of $72 < N < 80$ nuclei, including a triaxially deformed transition region near $N = 76$.^{6,7,10-13}

To throw additional light on these topics, we have undertaken a systematic study of the β/γ ,¹⁴ and β -delayed proton¹⁵ decays of nuclides near $Z = 64$ and close to the proton dip line, using mass-separated sources produced

by (HI, $xnyp$) reactions. Radioactive β -decay studies offer advantages over in-beam spectrometry for the assignment of ground-state spins, the identification of long-lived isomeric states, and the spectroscopy of high multipolarity γ transitions. Some examples of the use of radioactive decay data to address the problem of shape changes in neutron deficient rare-earth nuclides can be found in the work of Kern *et al.*⁶ and of Redon *et al.*¹⁶

In the present paper, we report our results for the $A = 141$ isobaric chain, including detailed level schemes for ^{141}Tb and ^{141}Gd , as well as the identification of a 24.5 s, β decaying, $\frac{11}{2}^-$ isomer in ^{141}Gd , with an 11% isomeric transition (IT) branch. Some preliminary results of this study, including the identification of the new isotopes ^{141}Dy (0.9 s) and ^{141}Tb (3.5 s) were published elsewhere.^{14,15,17,18} We plan to publish complementary results on the adjacent even mass chains with $A = 140$ and $A = 142$ separately.

II. EXPERIMENTAL

The desired nuclides were produced by bombarding ^{92}Mo targets (enriched to 97.4%) with ^{54}Fe and ^{52}Cr beams from the Berkeley SuperHILAC (heavy-ion linear accelerator). The self-supporting metal foil targets, about 2-mg/cm² thick, were mounted inside the high-temperature surface ionization source of the OASIS (on-line apparatus for SuperHILAC isotope separation) on-line mass separator facility¹⁹ in a configuration optimized for low transverse velocity recoils from compound-nucleus reactions. After mass separation of the evaporation residues, a beam of the mass 141 reaction products was deflected by an electrostatic mirror to a shielded spectroscopy laboratory located ~ 4 m above the mass separator. There, the activity was deposited on a pro-

grammable moving tape which positioned it, in a user selectable time cycle, in the center of an array of β , γ , and charged particle detectors (see further). In the $A=141$ experiments reported here, tape cycles of 2.4, 4, 12.8, 40, and 128 s were used.

The heavy-ion beam energies (276 and 210 MeV at the center of the target for the ^{54}Fe and ^{42}Cr beams, respectively) were chosen to correspond to the peaks of the excitation functions for the production of the desired mass 141 species, as calculated with the ALICE (Ref. 20) evaporation code. Table I shows the calculated production cross sections of $A=141$ isobars for the two target-projectile combinations and projectile energies. Since the beam energy loss in our targets (typically 25–30 MeV) is comparable to the full width at half maximum (FWHM) of the calculated excitation functions, uncertainties in the calculation should have only a minor effect on the overall efficiency and optimization of the experiments. The beam intensities, limited by target integrity and ion source temperature, were in the range of 0.1–0.2 particle microamperes.

The identification of ^{141}Dy in these experiments^{17,18} shows that the sensitivity of the system is sufficient for the detection and study of products with submillibarn cross sections, in runs of about 24 h duration. In other mass chains, we have been able to measure rare-earth activities with half-lives shorter than 100 ms, such as 70 ms ^{155}Lu , proving the capability of the system to detect radioactive species in the tens of milliseconds range.

Table I lists no products with $Z > 66$ or $Z < 63$; ^{141}Er and ^{141}Ho can indeed be produced in the ^{54}Fe induced reaction, but with cross sections that are well below our detection limits. No ^{141}Sm (and lower Z) nuclei can be produced from the ^{92}Mo target directly. Production from heavier mass Mo impurities in the target is negligible, due to the high target enrichment and low bombarding energy. Thus, any measured ^{141}Sm activity must result from the β decay of ^{141}Eu . As shown in a subsequent section, this observation is of crucial importance in the establishment of genetic relations and the absolute intensity and branching ratio normalizations of our data.

The detector array used for the measurements consisted of a Si ΔE - E particle telescope and a hyperpure Ge (HPGe) detector facing the front (deposit) side of the tape, and of a 1-mm thick plastic scintillator and a 24% n -type Ge detector on the opposite side of the tape. A third Ge detector (n type, 52% efficiency), oriented at 90° to the other two, was placed ~ 4.5 cm from the radioac-

tive source. In the ^{52}Cr experiment series, the relative positions of the 24% and 52% Ge detectors were interchanged. The HPGe detector was used primarily as a high-resolution (~ 700 eV FWHM at 122 keV) x-ray spectrometer, but could also serve (with a parallel low-gain amplifier and in conjunction with the E detector of the particle telescope) as the E detector in a ΔE - E electron/positron spectrometer for endpoint measurements up to ~ 10 MeV. The close geometry Ge detector served as the main γ -ray spectrometer. However, since our Z assignment of the observed particle and γ decays is based primarily on coincident characteristic x rays, this detector was also used (with a separate parallel high-gain amplifier) as a second x-ray spectrometer. The 90° detector was used primarily for $\gamma\gamma$ coincidence measurements. Since the intensity of γ -ray peaks in the close-geometry detector is subject to large multiplicity-dependent summing effects, singles spectra taken with the 90° detector were used in some experiments for the normalization of relative transition intensities.

Coincidences between the various detectors were recorded event by event and monitored by on-line sorting with preselected gates; all events were tagged with a time signal relative to the beginning of a tape cycle for half-life information. Singles data were also taken with the main γ -ray and x-ray detectors in a multispectrum mode in which the tape cycle was divided into eight equal time intervals. These singles spectra were used for the determination of precise half-lives, transition energies, and intensities as well as for the identification of noncoincident isomeric transitions.

A modified version of the SAMPO code²¹ was used for the analysis of all γ spectra. An important feature of this version is the ability to resolve strongly overlapping K x-ray peaks from sources containing up to four adjacent- Z rare-earth x-ray emitters. The total electron capture (EC) branching for a given isobar could be determined from the $K\alpha$ and $K\beta$ intensities observed in the HPGe detector after subtraction of internal conversion contributions, and suitable corrections for fluorescence yields, and $I_{EC(K)}/I_{EC(\text{tot})}$. The positron branching was calculated from a multilinear analysis²² of the γ^\pm (511 keV) intensity (correcting for annihilation-in-flight and source geometry) with respect to the intensities of representative γ rays for each parent. The total decay strength for each isobar could then be normalized to the sum of the EC and β^+ intensities. Half-lives were extracted from multicomponent decay curves using the least-squares code CLSQ.²³

The OASIS mass separator was operated with a nominal mass resolving power of 880, which reduces source contamination by adjacent masses to negligible levels. The selected mass value is stabilized to ± 0.01 u using a feedback system controlled by a PDP 11/10 computer. To avoid transient effects, the 50-keV beam of particles from the mass separator is interrupted by a fast deflection circuit within about $1 \mu\text{s}$ of any malfunction or disturbance (high-voltage sparks, etc.). Indeed, in all our experiments on a variety of rare-earth mass chains over a period of several years, we found no evidence for contamination by neighboring masses. Background peaks in the singles spectra not attributable to the mass separated re-

TABLE I. Cross sections for the production $A=141$ isobars in the $^{54}\text{Fe}+^{92}\text{Mo}$ and $^{52}\text{Cr}+^{92}\text{Mo}$ reactions, calculated with the ALICE (Ref. 20) evaporation code.

Isotope	$^{54}\text{Fe}+^{92}\text{Mo}$ (276 MeV)	$^{52}\text{Cr}+^{92}\text{Mo}$ (210 MeV)
^{141}Dy	0.7 mb	0.1 mb
^{141}Tb	15 mb	11 mb
^{141}Gd	46 mb	100 mb
^{141}Eu	18 mb	100 mb

action products are usually quite low and readily identifiable: Natural γ sources (^{40}K , Th, and U decay series), γ -induced fluorescence in the support structure, detector and shielding materials (Au and Pb K x rays), and neutron activation products (^{28}Al , $^{71}\text{Ge}^m$, $^{75}\text{Ge}^m$). Stable rare-earth mass markers (e.g., ^{141}Pr for the $A=141$ experiments), placed as trace quantities in the ion source, were used to select the desired mass chain, with suitable corrections for the different mass defects of the radioactive species. We, therefore, consider the mass assignments of the observed transitions as very reliable. The Z assignments are based mostly on the observation of coincident characteristic K x rays, and are similarly unambiguous. Weaker lines and higher-energy transitions often cannot be seen in the coincidence spectra, and their half-life determination may be uncertain due to poor counting statistics, parent-daughter equilibria, and interference from partially resolved lines from other isotopes. Assignment errors, although rather improbable, may be possible in these cases.

III. RESULTS

A. $^{141}\text{Eu}^{g+m}$

The decay of the 40-s $^{141}\text{Eu}^g$ was thoroughly investigated by Deslauriers, Gujrathi, and Mark,²⁴ who were able to assign 49 γ lines between 200 and 2250 keV to this decay. Over 40 of these transitions were also observed in our experiments, and apart from minor differences in the relative intensities of a few γ rays, our results are in excellent agreement with the earlier data and will, therefore, not be presented in detail. However, from our Sm K x-ray and 511-keV annihilation radiation intensities (as described in Sec. II), we obtain $\text{EC}/\beta^+ = 0.22(2)$ for $^{141}\text{Eu}^g$ decay and an intensity of 9(2)% for the 394.0-keV transition, rather than the 14(3)% derived in Ref. 24 from the growth of the ^{141}Sm daughter. With this renormalization, and the data from Ref. 24, the β branch to the $\frac{3}{2}^+$ level at 1.58 keV increases from 59 to 73(5) %.

In the same paper,²⁴ the identification of a 3.3(3) s $\frac{1}{2}^-$ $^{141}\text{Eu}^m$ isomer, decaying by a 96.4-keV $E3$ transition to the 40-s $\frac{5}{2}^+$ ground state of ^{141}Eu , and by β decay primarily to the 176-keV $\frac{1}{2}^-$ level in ^{141}Sm was also reported. On the basis of the observed growth of the 196.9-keV γ ray, characteristic of the decay of 22.6-min $^{141}\text{Sm}^m$, a branching ratio of 67% for the β decay of the $^{141}\text{Eu}^m$ isomer was derived.²⁴ This branching ratio corresponds to an unusually low $\log ft$ value of 4.1 for the $\pi h_{11/2} \rightarrow \nu h_{11/2}$ β transition.

Our measurements confirm the 96.4-keV $E3$ IT decay of $^{141}\text{Eu}^m$ with a slightly shorter half-life of 2.7(3) s. We cannot, however, support the high β branch in the decay of this isomer. In the 4- and 12.8-s tape cycle experiments, the intensities of the 2.7 s component of the annihilation radiation and of the Sm K α x rays are too low for a direct determination of the $^{141}\text{Eu}^m$ β decay; such a low intensity is not compatible with a 67% β branch. Since, as mentioned above, ^{141}Sm can be produced in our experiments only through the decay of ^{141}Eu , the activity ratio of the 22.6-min $^{141}\text{Sm}^m$ and the 10.2-min $^{141}\text{Sm}^g$ is a

measure of the β/IT ratio in the decay of $^{141}\text{Eu}^m$. In the 128-s tape cycle experiment all the intermediate species leading to the ^{141}Sm isomers have essentially decayed, and the branching ratio can be extracted without detailed evaluation of the growth and decay of all the nuclides in the isobaric chain. From the measured intensities of the 196-keV (74% abundance in the decay of $^{141}\text{Sm}^m$) and of the 404- and 438-keV (42.5 and 38%, respectively, in the decay of $^{141}\text{Sm}^g$) γ rays, we derive a $^{141}\text{Sm}^m/^{141}\text{Sm}^g$ activity ratio (at saturation) of 0.124(6). The value of the β branch in the decay of $^{141}\text{Eu}^m$ that corresponds to this ratio depends on the relative amount of $^{141}\text{Eu}^g$ not resulting from IT decay of $^{141}\text{Eu}^m$, i.e., produced either directly in the reaction or by the decay of $^{141}\text{Gd}^{g+m}$. Assuming no independent production of $^{141}\text{Eu}^g$, and branching ratios of 2% for the feeding of $^{141}\text{Sm}^m$ from $^{141}\text{Eu}^g$ decay (Ref. 24, renormalized as mentioned earlier) and for the feeding of $^{141}\text{Sm}^g$ from $^{141}\text{Eu}^m$, we derive a lower limit of 11.3(5)% for the β branch in the decay of $^{141}\text{Eu}^m$. A more realistic estimate of the production of $^{141}\text{Eu}^g$, based on calculated²⁰ reaction cross sections (see Table I), an isomer ratio of 20 for the preferential production of high-spin isomers in heavy-ion reactions and decay data for ^{141}Gd and ^{141}Tb from this study (see Secs. IIIB and

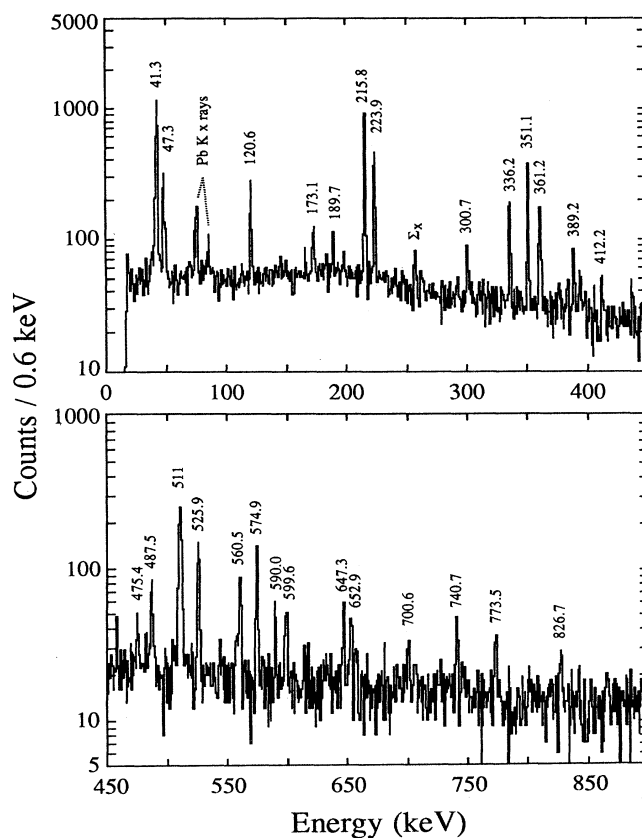


FIG. 1. Gamma-ray spectrum of ^{141}Gd decay gated on Eu K α x rays (40-s tape cycle). Peaks marked by energy identify transitions assigned to the decay of $^{141}\text{Gd}^{g+m}$. Peaks associated with the IT decay of $^{141}\text{Gd}^m$ do not appear in this spectrum.

III C), leads to a value of $13 \pm 4\%$ for the branching ratio. This result is quite insensitive to the assumptions regarding the decay of higher members of the chain, the isomer ratios, and the reaction cross sections; reasonable uncertainties associated with all three sources are included in the uncertainty estimate given above. The $\log ft$ value for the $\pi h_{11/2} \rightarrow \nu h_{11/2}$ transition corresponding to the 13% branching ratio and the decay scheme of Ref. 24 is 5.2(2), in good agreement with $\log ft$ systematics in this region.

This $\log ft$ assumes no feeding of higher excited levels in this decay; the true value is therefore expected to be somewhat higher.

B. $^{141}\text{Gd}^{g+m}$

The discovery of ^{141}Gd was first reported in a preliminary presentation of this work.^{17,18} Concurrently, Redon *et al.*¹⁶ determined a ^{141}Gd half-life of 22(3) s, assigned

TABLE II. Transition energies, level assignments, and relative intensities for $^{141}\text{Gd}^{g+m}$. The β^+ and EC strengths for $m+g$ decay were $I_{\beta^+} = 550(140)$ and $I_{\text{EC}} = 200(40)$, relative to $I_{351.1} = 100$.

E (keV) ^a	Level	I (Rel) ^{b,c}	E (keV) ^a	Level	I (Rel) ^{b,c}
Eu ^d $K\alpha_2$		73(7)	525.9 ^h (2)	525.9	35 ^k (6)
Eu ^d $K\alpha_1$		146(15)	526.0(2)	622.5	19 ^k (5)
Eu ^d $K\beta_1$		49(5)	544.3(1)		5(2)
Eu ^d $K\beta_2$		14(3)	557.5(1)		5(2)
Gd ^e $K\alpha_2$		10(2)	560.5(1)	656.7	27(3)
Gd ^e $K\alpha_1$		20(2)	574.9(1)	671.7	57(6)
Gd ^e $K\beta_1$		6(2)	590.0(1)	1047.4	13(2)
Gd ^e $K\beta_2$		2(1)	599.6(1)	1047.4	12(2)
59.8 ^f (1)	258.2	5(2)	647.3(1)	967.7	23(2)
85.2 ^f (1)	198.4	3(1)	652.9(1)	749.4	21(2)
96.4 ^g (1)	96.5	13(2)	657.0(2)		4(2)
113.2 ^f (1)	113.2	9(2)	700.6(1)		8(2)
119.6 ^f (1)	377.8	5(2)	740.7(1)	837.1	18(2)
120.6 ^h (1)	336.2	19(2)	746.4(1)		7(2)
145.0 ^f (1)	258.2	6(2)	773.5(1)	869.9	15(2)
173.1 ^h (1)	509.3	6(2)	826.7(1)	923.2	9(2)
189.7 ^h (1)	525.9	7(2)	841.4(1)		7(2)
198.4 ^f (1)	198.4	27(3)	864.4(1)		6(2)
215.8 ^h (1)	215.8	111(12)	972.2(1)	2019.6	10(2)
223.9(1)	320.4	72(7)	976.2(1)	1072.6	9(2)
258.2 ^f (1)	258.2	23(2)	1036.4(1)		4(2)
293.3 ^h (2)	509.3	4 ⁱ (2)	1072.6 ^{h,1} (2)	1408.6	2(1)
300.7(1)	923.2	10(2)	1072.6(2)	1072.6	2(1)
336.2 ^h (1)	336.2	35(4)	1097.6(1)		12(2)
351.1(1)	447.8	100(10)	1148.5(1)	1820.4	5(2)
361.2(1)	457.6	42(4)	1164.0(1)	1820.4	5(2)
389.2(1)	837.1	14(2)	1172.2(1)		6(2)
412.2(1)	869.9	13(2)	1192.8 ^h (1)	1408.6	14(2)
457.6(1)	457.6	9(2)	1338.0(2)	1795.7	6(3)
475.4(1)	923.2	13(2)	1348.0(2)	1795.7	6(2)
487.5(1)		12(2)	1397.2(2)		9(2)
509.0(5)	509.3	j	1922.8(2)	2019.6	6(2)

^aAssigned to decay of $^{141}\text{Gd}^m$ to levels in ^{141}Eu , except where noted.

^bIntensity relative to $I_{351.1} = 100$.

^cFor absolute intensity per 100 decays of $^{141}\text{Gd}^m$, multiply by 0.138.

^dPrompt x rays only. Conversion of 96.4-keV $E3$ IT decay of $^{141}\text{Eu}^m$ not included.

^eFrom conversion of IT decay of $^{141}\text{Gd}^m$.

^fFrom IT decay of $^{141}\text{Gd}^m$. For absolute intensity per 100 $^{141}\text{Gd}^m$ decays, multiply by 0.138.

^gFrom IT decay of $^{141}\text{Eu}^m$.

^hAssigned to $^{141}\text{Gd}^g$ decay. For absolute intensity per 100 $^{141}\text{Gd}^g$ decays, multiply by 0.48.

ⁱSeen only in coincidence.

^jMasked by 511-keV annihilation radiation.

^kThe 526-keV intensity divided between the 525.9 \rightarrow 0 and the 622.4 \rightarrow 96.4 transitions on the basis of coincidence data and γ intensity balance.

^lBy energy difference, the 1072.6(2) γ ray can fit both the 1072.6 \rightarrow 0 transition in $^{141}\text{Gd}^m$ decay and the 1408.6 \rightarrow 336.2 transition in $^{141}\text{Gd}^g$ decay. The intensity is apportioned equally.

six γ rays to its decay and placed them in a tentative decay scheme. More recently, Turcotte *et al.*²⁵ proposed rather detailed and extensive decay schemes for 20.8(8) s $^{141}\text{Gd}^m$ (β and IT) and 1.3(7) s $^{141}\text{Gd}^g$. These decay schemes comprise 45 γ transitions between 28 excited levels in ^{141}Eu , as well as four levels and six transitions in ^{141}Gd associated with the IT decay of $^{141}\text{Gd}^m$. There is substantial overlap between the data of Ref. 25 and our results, but there are also some major differences.

Figure 1 shows a coincident γ spectrum gated on the Eu $K\alpha$ x rays, obtained in a 40-s tape cycle experiment. The high resolution of the detector and good statistics of the data permit an unambiguous identification and assignment of more than 30 transitions to the decay of ^{141}Gd . Some additional (relatively weak or high-energy) γ rays were assigned to this decay on the basis of suitably gated coincidence spectra, half-lives, and energies matching the level scheme established by the other lines. Table II lists all of the γ rays we attribute to transitions in ^{141}Eu following the β decay of ^{141}Gd , along with their relative intensities and level scheme placements. Coincident γ rays observed in spectra gated on the relatively intense peaks are listed in Table III.

Table II also includes rather strong γ transitions at 59.8, 85.2, 113.2, 119.6, 145.0, 198.4, and 258.2 keV that are not seen in Fig. 1. A coincidence spectrum gated on the Gd $K\alpha$ x rays shown in Fig. 2 clearly identifies these lines as transitions in ^{141}Gd . Since their half-life is the same, within statistical errors, as that of the prominent γ rays associated with the β decay of ^{141}Gd , we have assigned these transitions¹⁴ to an IT cascade from the $\frac{11}{2}^-$ isomeric level at 377.8 keV to the $\frac{1}{2}^+$ ground state of ^{141}Gd . The 119.6-keV γ ray is the only one of the seven transitions in the cascade that is not also seen in the decay of 3.5-s ^{141}Tb , and is clearly the $E3$ transition to the $\frac{5}{2}^+$ state at 258.2 keV. The placement of the intermedi-

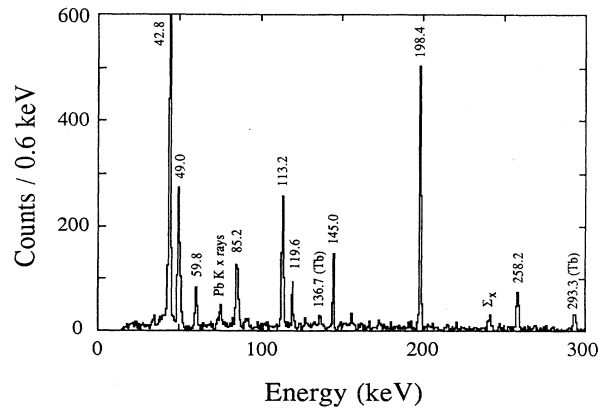


FIG. 2. Gamma-ray spectrum of ^{141}Gd decay gated on Gd $K\alpha$ x rays (40-s tape cycle). Unless marked otherwise, all the peaks are associated with the IT decay cascade of $^{141}\text{Gd}^m$.

ate levels at 198.4 and 113.2 keV is based on coincidence relationships and intensity balances of the γ rays in the cascade. The $J^\pi = \frac{3}{2}^+$ assignment to these levels is based on level systematics of $N=77$ nuclei, shown in Fig. 3. This sequence of levels seems to be more in line with the trends established by the other three isotones than that

TABLE III. Gamma-gamma coincidences observed in $^{141}\text{Gd}^{g+m}$ decays.

Gate	Coincident gamma rays
Eu K x rays	121, 173, 190, 216, 224, 293, 301, 336, 351, 361, 389, 412, 458, 475, 487, 526, 544, 560, 575, 590, 600, 647, 653, 701, 741, 773, 827
Gd K x rays	60, 85, 113, 120, 145, 198, 258
60	85, 113, (120), 198
85	60, 113, 120
113	60, 85, 120, 145
121	173, 190, 216
145	113, 120
198	60, 120
216	120, 173, 190, (293)
224	488, 647
258	120
336	190
351	389, 475, 600
361	412, 590
389	351
526	301

$\frac{11}{2}^-$ 520			
1.6 s			
$\frac{11}{2}^-$ 447		$\frac{11}{2}^-$ 457	
20 s		10 s	
			$\frac{11}{2}^-$ 378
			24 s
$\frac{3}{2}^+$ 296	$\frac{5}{2}^+$ 286	$\frac{5}{2}^+$ 267	$\frac{5}{2}^+$ 258
$\frac{5}{2}^+$ 296	$\frac{3}{2}^+$ 269	$\frac{3}{2}^+$ 223	$\frac{3}{2}^+$ 198
	$\frac{3}{2}^+$ 109	$\frac{3}{2}^+$ 112	$\frac{3}{2}^+$ 113
$\frac{3}{2}^+$ 83			
$\frac{1}{2}^+$ 0	$\frac{1}{2}^+$ 0	$\frac{1}{2}^+$ 0	$\frac{1}{2}^+$ 0
$^{135}_{58}\text{Ce}_{77}$	$^{137}_{60}\text{Nd}_{77}$	$^{139}_{62}\text{Sm}_{77}$	$^{141}_{64}\text{Gd}_{77}$

FIG. 3. Systematics of the first four excited levels of neutron deficient $N=77$ nuclides. Data for ^{141}Gd from this work, ^{139}Sm data from Ref. 31, and ^{137}Nd and ^{135}Ce data from Ref. 28.

proposed by Turcotte *et al.*,²⁵ who place the two $\frac{3}{2}^+$ levels at 60 and 145 keV, respectively. Recently, Béraud *et al.*²⁶ in an analysis of their own data confirmed our interpretation.

In the 128-s tape cycle experiment, the decay of the most prominent of the γ rays assigned to the IT and β decays of ^{141}Gd could be followed for well over three half-lives, allowing an accurate and reliable determination of their half-life. Most of these γ rays had a half-life of 24 s. Since the 96.4-keV isomeric decay of the $\frac{11}{2}^-$ $^{141}\text{Eu}^m$ (in equilibrium with its parent) as well as transitions associated with the IT decay of $^{141}\text{Gd}^m$ are included in this group, the 24-s activity is identified as the $\frac{11}{2}^-$ isomer, $^{141}\text{Gd}^m$. From a weighted average of 8 γ rays (some seen independently in two detectors), a half-life of 24.5(5) s is adopted.

The prominent 215.8-keV γ ray, however, had a significantly shorter apparent single-component half-life. This is illustrated in Fig. 4, which shows the decay of the 215.8- and 223.9-keV γ rays. Based on this difference, clearly outside statistical error margins, we assign the 215.8-keV line to the decay of the $\frac{1}{2}^+$ $^{141}\text{Gd}^g$. Using coin-

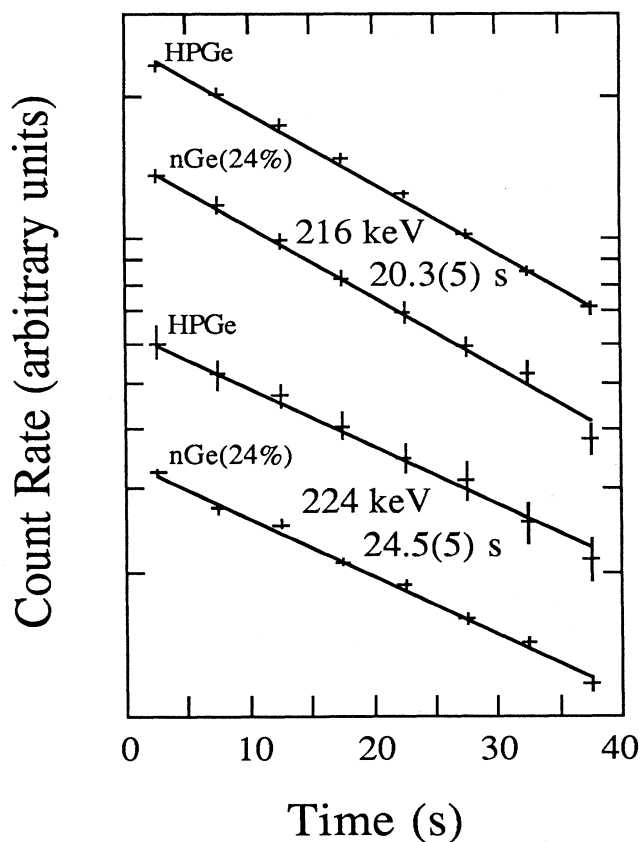


FIG. 4. Decay curves of the 216- and 224-keV γ rays populated in ^{141}Gd decay, taken with two different detectors. Differences in slope outside statistical error margins are clearly visible.

idence data and energy differences, several additional γ rays were assigned to this decay. Also, the ~ 20 s delayed proton activity observed in the decay of ^{141}Gd was attributed to $^{141}\text{Gd}^g$ on the basis of the observed final-state feedings in the delayed proton decay daughter ^{140}Sm ,²⁷ and a delayed proton branch of 0.03(1)% was determined.

As can be seen from Fig. 4, the single component half-life of $^{141}\text{Gd}^g$ appears to be about 20 s, i.e., very close to that of $^{141}\text{Gd}^m$. The apparent single-component half-life of the 215.8-keV γ ray extracted from the 40-s tape cycle experiment is 20.3(5) s, while the value extracted from the 128-s cycle is 22.1(5) s. Similar discrepancies are also exhibited by the 336.2-keV γ ray [18.6(9) s and 23.3(9) s, respectively] and by the β -delayed protons [16(4) s and 23(3) s, respectively]; they can be explained by differences in the relative contribution of $^{141}\text{Gd}^g$ produced directly, and by decay of ^{141}Tb and $^{141}\text{Gd}^m$ between the ^{54}Fe and ^{52}Cr induced reactions used, respectively, in the two experiments. From a growth-decay analysis of transitions assigned to the decay of $^{141}\text{Gd}^g$ in the 128-s cycle experiment, we determined a half-life value of 14(4) s for $^{141}\text{Gd}^g$. In our 2.4- and 4-s tape cycle data we see no evidence of a short-lived component that would be consistent with the 1.3(7) s half-life claimed by Turcotte *et al.*²⁵ A similar conclusion was also reached by Béraud *et al.* in Ref. 26.

Using energy differences, intensity balances, and coincidence data, all γ rays could be uniquely assigned to either the ground-state or isomeric-state decays of ^{141}Gd , and partial decay schemes for both isomers are shown in Fig. 5. The total β decay strength from the sum of the EC and β^+ intensities could be determined only for the combined $^{141}\text{Gd}^m+g$ decay. Relative to $I_{351.1} = 100$, the β^+ and EC strengths were $I_{\beta^+} = 550(140)$ and $I_{\text{EC}} = 200(40)$. However, the sum of the γ -ray intensities (corrected for internal conversion) in the ^{141}Eu daughter agreed well with the aggregate β strength, so the low- and high-spin normalizations could be determined from the sum of the γ -ray intensities feeding the $\frac{5}{2}^+$ ground state and the 96.5-keV $\frac{11}{2}^-$ isomeric state, respectively. From the decay scheme, the branching for IT decay was determined to be 11(2)%. The double placement of the 526-keV γ ray is supported by intensity considerations and coincidence with the 301-keV transition. The double placement of the 1073-keV γ ray is based on energy differences alone. The major difference between our scheme and that of Ref. 25 is the placement of the 216-keV transition, and the resulting assignment and identification of low-spin levels.

C. ^{141}Tb

For the study of the decay of ^{141}Tb , we used the data from the 4- and 12.8-s tape cycles. A coincident γ -ray spectrum gated on Gd $K\alpha$ x rays is shown in Fig. 6. Due to the lower production cross section (see Table I), the counting statistics are appreciably lower than in the case of ^{141}Gd decay. However, peaks associated with the decay of ^{141}Tb can be clearly identified. A list of 36 γ rays between 50 and 650 keV that we have assigned to this de-

cay is presented in Table IV. Most of these γ rays exhibit a single-component decay behavior with a weighted average half-life of 3.5(2) s. Six of the transitions associated with the IT decay of 24.5-s $^{141}\text{Gd}^m$ (see Sec. III B) also have a 3.5-s component. This shows that the low-lying, spin $\frac{5}{2}^+$ and $\frac{3}{2}^+$ states at 258, 198, and 113 keV are populated quite strongly in the decay of ^{141}Tb . Gamma-gamma coincidences seen with various gates are listed in Table V. Using these coincidence relationships along with energy differences and intensity balances, almost all the observed γ transitions can be placed in a level scheme

comprising 16 excited levels in ^{141}Gd , shown in Fig. 7. This level scheme reproduces and considerably expands the scheme recently proposed by Béraud *et al.*²⁶ The γ transitions included in the decay scheme (after corrections for internal conversion) account for $\sim 85\%$ of the total β strength [$I_{\beta^+} = 425(100)$ and $I_{\text{EC}} = \sim 250$, relative to $I_{293.3} = 100$] associated with the decay of ^{141}Tb . In view of the high Q value, some unobserved feeding of higher-lying levels should be expected, however, intensity balance through the first six excited levels indicates that the intensity of transitions not included in the scheme is

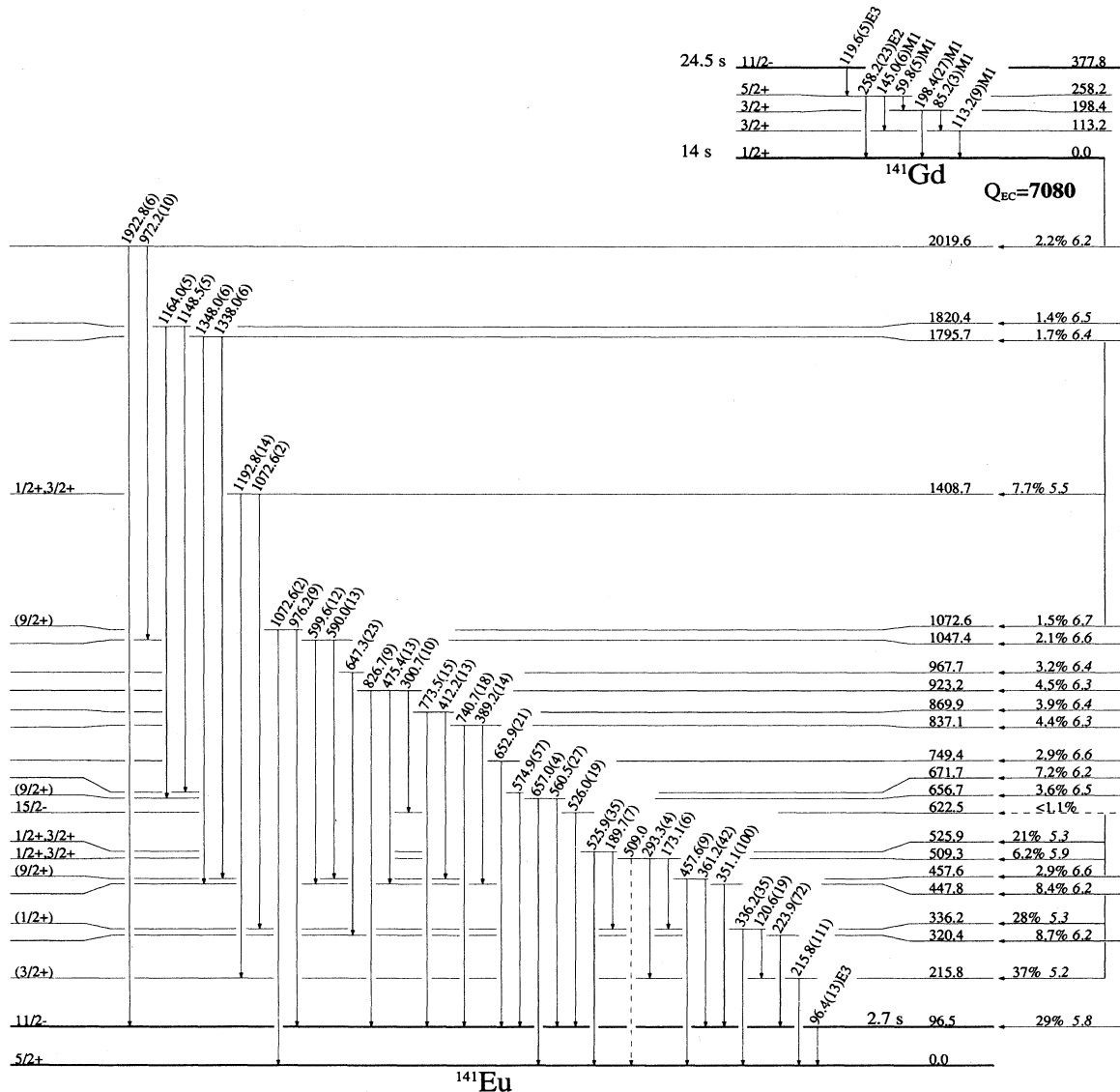


FIG. 5. Decay scheme for the decay of $^{141}\text{Gd}^{g+m}$ to levels in ^{141}Eu . The level energies have been calculated from a least-squares fit of the γ -ray energies to the level scheme. The intensities given in parentheses for each transition are relative photon intensities and are not corrected for internal conversion. For absolute γ intensities per 100 decays of $^{141}\text{Gd}^m$ or $^{141}\text{Gd}^g$, multiply by 0.138 or 0.48, respectively. The $\log ft$ values were calculated without taking into account unobserved transitions to higher-lying levels; actual $\log ft$ values are therefore expected to be lower by 0.1–0.2. Except for the IT decay cascade, spin and parity assignments are tentative, based on β and γ selection rules. The Q_{EC} value is from S. Liran and N. Zeldes, *At. Data Nucl. Data Tables* 17, 431 (1976).

low. These intensity considerations leave little room for significant direct β feeding of either the $\frac{1}{2}^+$ ground state or the 377.8-keV $\frac{11}{2}^-$ isomeric level in ^{141}Gd , as would be expected if the postulated^{25,26} $\frac{1}{2}^+$, $\frac{11}{2}^-$ spin assignments for ^{141}Tb were indeed correct. Turcotte *et al.*²⁵ claim to have observed the low-spin member of the isomeric pair with a half-life of 7.9(6) s. We see no indication of this longer half-life; within statistical uncertainties, all the γ rays we assign to ^{141}Tb decay with a single half-life of 3.5 s, and we are unable to separate our decay scheme into low- and high-spin branches.

It can be seen that both high- and low-spin levels in ^{141}Gd appear to be populated with comparable intensity in the decay of ^{141}Tb . In particular, the levels at 551.6 and 895.2 keV, fed by low $\log ft$ β transitions, deexcite through $\frac{5}{2}^+$ and $\frac{11}{2}^-$ levels, and the 752.6-keV level, also fed by a low $\log ft$ transition, deexcites through a $\frac{3}{2}^+$ level. This is only consistent with a J^π assignment of $\frac{5}{2}^-$ or $\frac{7}{2}^-$ for the ^{141}Tb parent. Based on a consideration of available Nilsson model states (see further) we propose a spin of $\frac{5}{2}^-$ for the ground state of ^{141}Tb .

The experimental situation in ^{141}Tb differs from that seen by Redon *et al.*¹⁶ in the decay of ^{143}Tb . A strong β feeding of the 45-keV, $\frac{3}{2}^+$ first-excited state of ^{143}Gd is

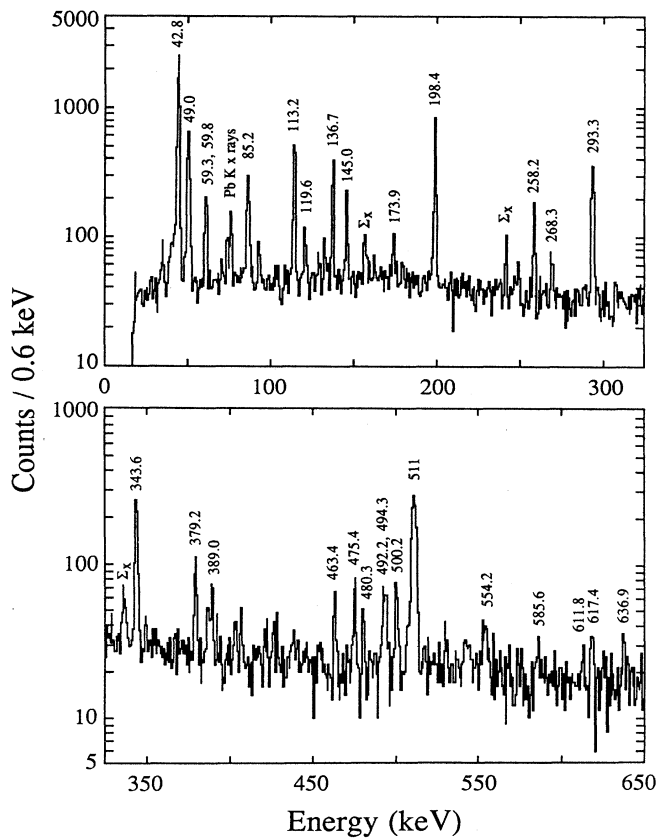


FIG. 6. Gamma-ray spectrum of ^{141}Tb decay gated on Gd $K\alpha$ x rays (4-s tape cycle). Peaks marked by energy identify transitions assigned to the decay of ^{141}Tb .

also observed, indicating a positive parity for the ground state of ^{143}Tb , to which the authors assign a spin of $\frac{5}{2}^+$. Redon *et al.*¹⁶ also postulate the existence of an $\frac{11}{2}^-$ isomer, which is expected from systematics, but for which there is no compelling evidence in the data. It is quite likely that in both ^{141}Tb and ^{143}Tb the excitation energy of the $\frac{11}{2}^-$ level is such that there is no long-lived isomeric state.

TABLE IV. Transition energies, level assignments, and relative intensities for ^{141}Tb . The β^+ decay strength is 425(100) and the EC strength is ~ 250 , relative to $I_{293.3} = 100$.

E (keV) ^a	Level	I (rel) ^{b,c}
Gd $K\alpha_2$		133(13)
Gd $K\alpha_1$		241(24)
Gd $K\beta_1$		74(7)
Gd $K\beta_2$		20(2)
59.3(1)	551.6	18(4)
59.8 ^d (1)	258.2	10(2)
85.2 ^d (1)	198.4	11(2)
91.5(1)	752.6	2(1)
94.5(1)	646.1	1(1)
113.2 ^d (1)	113.2	47(5)
119.6 ^e (1)	377.8	e
131.6(1)	646.1	47(5)
136.7(1)	514.4	85(9)
145.0 ^d (1)	258.2	22(3)
173.9(1)	551.6	15(2)
198.4 ^d (1)	198.4	88(9)
206.7(2)	758.3	4(3)
234.5(1)	492.3	5(2)
248.8(1)	895.2	5(2)
258.2 ^d (1)	258.2	70(7)
268.3(2)	646.1	29(3)
293.3(1)	551.6	100(10)
343.6(1)	895.2	97(10)
379.2(1)	492.3	29(3)
389.0(1)	940.5	11(2)
402.9(1)	895.2	28(7)
406.8(1)		8(2)
426.0(1)	940.5	7(2)
463.4(1)	661.4	22(3)
475.4(1)	989.7	51(5)
480.3(1)		32(3)
492.2(1)	492.3	41(4)
494.3(1)	752.6	40(4)
500.2(1)	758.3	54(5)
517.5(1)	895.2	27(3)
530.9(2)		15(2)
554.2(1)	752.6	20(2)
585.6(1)	1100.0	21(2)
611.8(1)	989.7	8(2)
617.4(1)	1131.8	28(3)
636.9(1)	895.2	11(2)

^aAssigned to decay of ^{141}Tb , except where noted.

^bIntensity relative to $I_{293.3} = 100$.

^cFor absolute intensity per 100 decays of ^{141}Tb , multiply by 0.168.

^dAlso in $^{141}\text{Gd}^m$ IT decay. Intensity corrected to include only the 3.5 s component from ^{141}Tb decay.

^eIT decay of $^{141}\text{Gd}^m$.

TABLE V. Gamma-gamma coincidences observed in ^{141}Tb decays.

Gate	Coincident gamma rays
Gd K x rays	59, 60, 85, 92, 113, 120, 132, 137, 145, 174, 198, 249, 258, 268, 293, 344, 379, 389, 403, 407, 426, 463, 475, 480, 492, 500, 531, 554, 586, 617, 637
59+60	85, 113, 198, 293, 344, 379, 492
85	60, 113, (120), 293, 344, 389, 554
113	59, 60, 85, 120, 145, 293, 344, 379, 494, 554
137	132, 426, 475, 586
145	113, 293, 344
198	60, 293, 344, 463, 500, 554
258	120, 293, 344, 500, 637
293	60, 85, 113, 145, 198, 258, 344, 389
344	60, 85, 113, 145, 174, 198, 258, 293
379	113

D. ^{141}Dy

Due to its low production cross section, we could study in detail only the delayed proton branch in the decay of this isotope. As reported in Refs. 14, 15, and 18, the half-life of ^{141}Dy is 0.9(2) s. No γ rays following its β decay were previously identified, but transitions of 307.3, 503.8, and 647.5 keV in the daughter ^{141}Tb are now known from in-beam work by Goettig *et al.*¹⁰ We observed Tb $K\beta_1$ x rays and two, very weak γ rays at 53.0(1) and 307.3(2) keV in the 2.4- and 4-s tape cycle data with short (< 1 s) half-lives and have tentatively assigned these transitions to ^{141}Dy β decay. Feedings of final states in ^{140}Gd observed in the delayed proton decay of ^{141}Dy (specifically the intensity ratio of the $4^+ \rightarrow 2^+$ and $2^+ \rightarrow 0^+$ transitions) are not consistent with a single low spin ($\frac{1}{2}^+$) or high-spin ($\frac{11}{2}^-$) precursor.²⁷ The data can be reconciled by assuming contributions from both spins²⁷ or by postulating a single intermediate spin value of $\frac{7}{2}^-$ or $\frac{9}{2}^-$ for the ^{141}Dy precursor. On the basis of

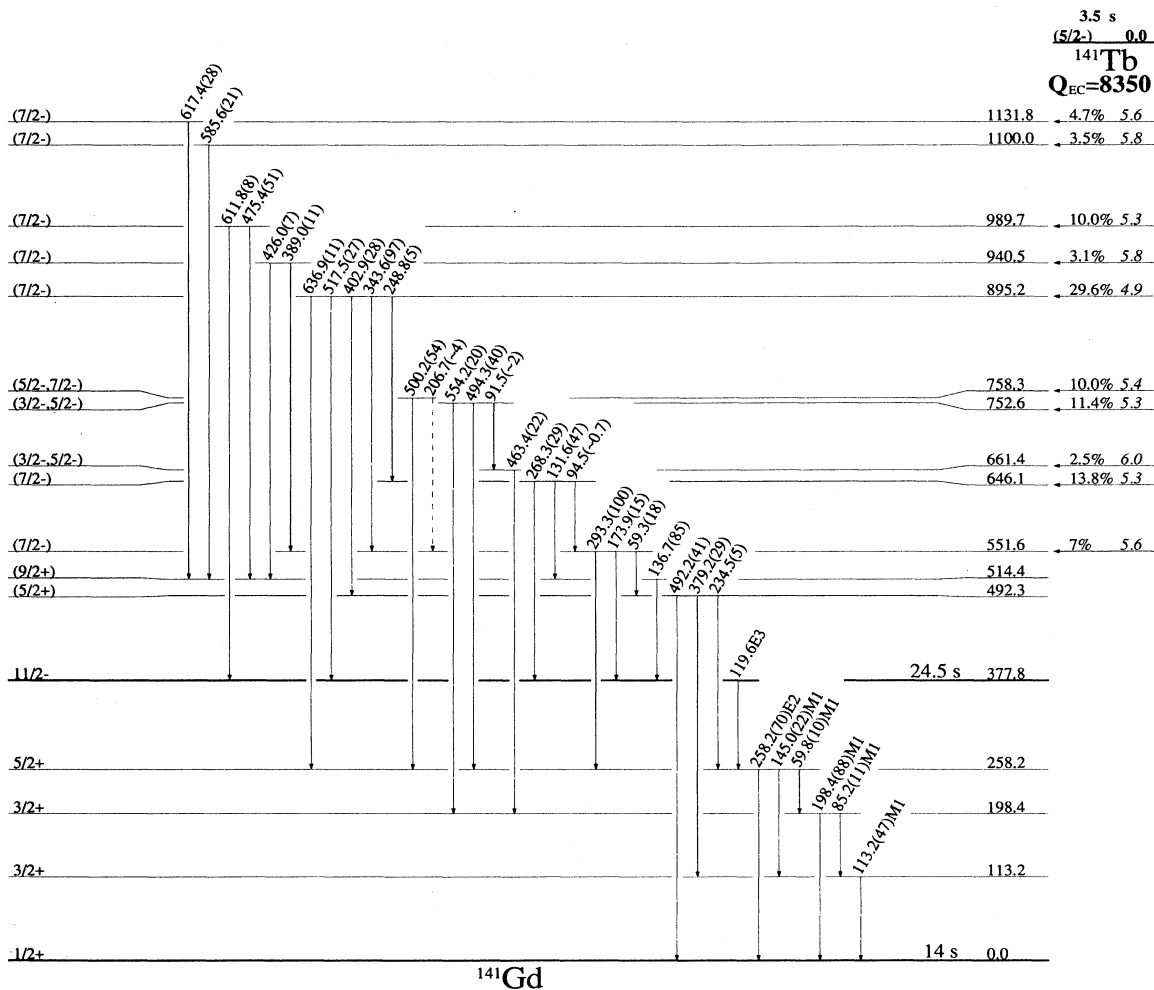


FIG. 7. Decay scheme for the decay of ^{141}Tb to levels in ^{141}Gd . The level energies have been calculated from a least-squares fit of the γ -ray energies to the level scheme. The intensities given in parentheses for each transition are relative photon intensities; multiply by 0.168 for absolute γ intensities per 100 ^{141}Tb decays. The $\log ft$ values were calculated without taking into account unobserved transitions to higher lying levels; actual $\log ft$ values are therefore expected to be lower by 0.1–0.2. Spin and parity assignments are tentative, based on β and γ selection rules. The Q_{EC} value is from S. Liran and N. Zeldes, *At. Data Nucl. Data Tables* 17, 431 (1976).

available Nilsson states (see following) we suggest a J^π of $\frac{9}{2}^-$ for ^{141}Dy . This would be in agreement with the systematics of the lighter $N=75$ isotones ^{131}Ba ,²⁸ ^{133}Ce ,²⁸ and ^{135}Nd ,²⁹ where $\frac{1}{2}^+$, $\frac{9}{2}^-$ isomer pairs have been seen, and with ^{137}Sm (Refs. 16 and 30) and ^{139}Gd (Ref. 13) where $\frac{9}{2}^-$ states have been observed.

IV. SUMMARY AND CONCLUSIONS

We have presented and interpreted experimental data on the β/γ decay of $^{141}\text{Eu}^m$, $^{141}\text{Gd}^{g+m}$, ^{141}Tb , and ^{141}Dy . What conclusions can be drawn from this body of data with regard to the fundamental nuclear structure questions of shape changes and disappearance of the $Z=64$ shell below $N=78$? For ^{141}Eu , our data confirm previously published results;²⁴ the amended $\log ft$ value of 5.2(2) for the $\pi h_{11/2} \rightarrow \nu h_{11/2}$ β transition from $^{141}\text{Eu}^m$ removes an apparent anomaly in $\log ft$ systematics in the $50 < Z, N < 82$ region. The $B(E3)$ value for the 96.4-keV $\frac{11}{2}^- \rightarrow \frac{5}{2}^+$ isomeric transition is 0.8 Weisskopf units (W.u.). This lack of hindrance is indicative of the single-particle nature of the relevant $Z=63$ proton levels.

The low-lying, low-spin levels in ^{141}Gd , as well as the position of the $\frac{11}{2}^-$ isomeric state, follow closely the systematics established by the $N=77$ isotones of lower Z (see Fig. 3). The lack of $Z=64$ shell closure effects should not, however, be construed as evidence for the disappearance of the closure, since the $N=81$ level systematics from Ce to Gd also exhibit a smooth sequence (see Fig. 13 of Ref. 16). The $B(E3)$ value of the 119.6-keV $\frac{11}{2}^- \rightarrow \frac{5}{2}^+$ isomeric transition is only 8×10^{-4} W.u., which is about 5–10 times slower than the measured rate in the other three isotones.³¹ This additional hindrance may be related to shape differences or to residual effects of the $Z=64$ shell. The increase of the energy gap between the $\frac{11}{2}^-$ and $\frac{1}{2}^+$ states between $N=79$ and $N=77$ in Ce, Nd, and Sm nuclei has been attributed to changes in deformation near $N=77$.¹⁶ We observe a very similar increase of the energy gap in Gd, again indicating no appreciable effect of the $Z=64$ shell closure.

For ^{141}Tb , our ground-state J^π assignment of $\frac{5}{2}^-$ deviates from the previously assumed $\frac{11}{2}^-$ ground state (or $\frac{11}{2}^-$, $\frac{1}{2}^+$ isomeric pair).^{25,26} This assumption is based on an extrapolation from heavier (spherical) Tb nuclides. Figures 8(a) and (b) show Nilsson-type level diagrams for protons and neutrons, respectively, in the appropriate Z and N regions, based on the folded Yukawa potential.³² For a spherical nucleus, $\frac{11}{2}^-$ is indeed the most probable ground-state spin for $Z=65$. For deformations in the $\epsilon_2=0.1$ – 0.2 range, the preferred candidate for the Fermi level of Tb is the $\frac{5}{2}^-$ [532] state of the $h_{11/2}$ orbital [Fig. 8(a)], in excellent agreement with the decay scheme of Fig. 7. A $\frac{7}{2}^-$ assignment, also compatible with the data, is ruled out by the lack of suitable candidates in the Nilsson diagram.

The $\frac{5}{2}^+$ assignment for the ground state of ^{143}Tb (Ref. 16) is more difficult to justify on the basis of the Nilsson diagram of Fig. 8(a). However, the energy of the $\frac{5}{2}^+$ [402] state increases rapidly with deformation; at

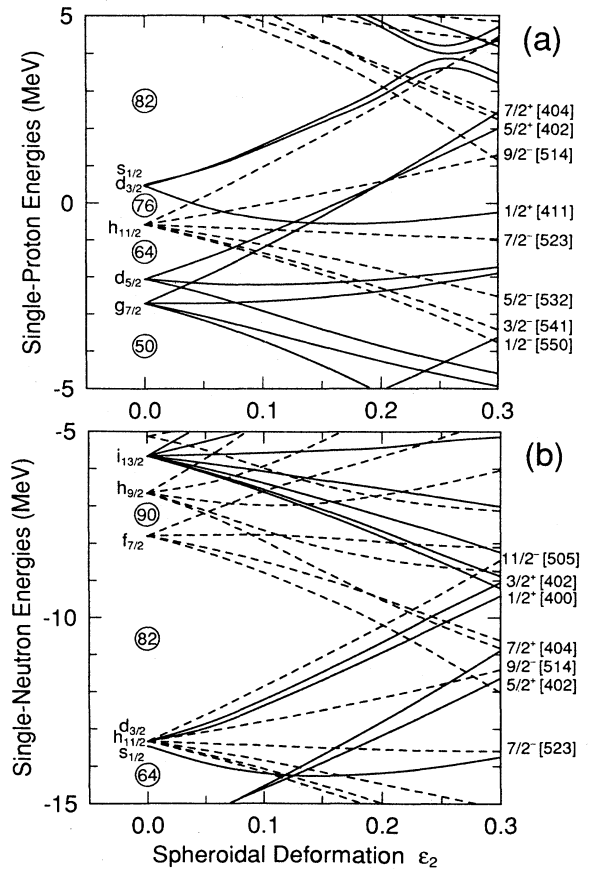


FIG. 8. Proton (a) neutron (b) single-particle level energies for ^{141}Dy as a function of spheroidal deformation, based on the Nilsson model with a folded Yukawa potential described in Ref. 32. In the calculations, the range of the Yukawa function was $a_p = a_n = 0.80$ fm and the proton and neutron spin-orbit interaction strengths were $\lambda_p = 31.52$ and $\lambda_n = 34.14$, respectively. A constant $\epsilon_4 = 0.04$ was assumed.

$\epsilon_2 \sim 0.1$, its energy is very close to that of four or five other states, so that the possibility of it becoming the ground state is not excluded by the Nilsson diagram.

Turning to the neutron diagram [Fig. 8(b)], we find that the $\frac{9}{2}^-$ [514] state of the $h_{11/2}$ orbit is an obvious Fermi level candidate for the $N=75$ ^{141}Dy , over a wide range of deformations. This is in good agreement with our interpretation of experimental results in Sec. III D. The $\frac{9}{2}^-$ J^π assignment for ^{141}Dy is further supported by the systematics of the other $N=75$ isotones. This may be another example of a relatively abrupt onset of shape changes near $N=76$, or of the softness of nuclei in this region.

In conclusion, the results reported in this paper provide ample evidence for the occurrence of shape changes and for the disappearance of the $Z=64$ shell gap below $N=78$. The overall consistence of ground-state J^π assignments with the Nilsson level diagrams of Fig. 8, suggests prolate deformations, in agreement with theoretical predictions. Unfortunately, the data from a single mass chain are not sufficient to search for signatures of triaxi-

ality, or for other far-reaching conclusions. Further β -decay studies of other mass chains in this poorly characterized transitional region are necessary to establish the systematics from which deeper nuclear structure insights can be obtained.

ACKNOWLEDGMENTS

One of us (J.G.) would like to thank the Lawrence Berkeley Laboratory (LBL) for its hospitality during the

course of this work. We would also like to express our thanks to Peter Möller for performing the Nilsson model calculations and for helpful discussions, and to Kari Vierinen for his interest and assistance. The excellent technical support and efficient cooperation of the LBL SuperHILAC staff and of L. F. Archambault and A. A. Wydler are gratefully acknowledged. This work was supported by the U.S. Department of Energy under Contract DE-AC03-76SF00098.

*On leave of absence from the Soreq Nuclear Research Center, Yavne 70600, Israel.

- ¹I. Ragnarsson, A. Sobczewski, R. K. Sheline, S. E. Larsson, and B. Nerlo-Pomorska, Nucl. Phys. **A233**, 329 (1974).
- ²I. Ragnarsson and R. K. Sheline, Phys. Scr. **29**, 385 (1984).
- ³G. A. Leander and P. Möller, Phys. Lett. **110B**, 17 (1982).
- ⁴J. Meyer-Ter-Vehn, Nucl. Phys. **A249**, 111 (1975); **A249**, 141 (1975).
- ⁵J. A. Cizewski and E. Gülmez, Phys. Lett. B **175**, 11 (1986).
- ⁶B. D. Kern, R. L. Mlekodaj, G. A. Leander, M. O. Kortelahti, E. F. Zganjar, R. A. Braga, R. W. Fink, C. P. Perez, W. Nazarewicz, and P. B. Semmes, Phys. Rev. C **36**, 1514 (1987).
- ⁷N. Redon, J. Meyer, M. Meyer, P. Quentin, P. Bonche, H. Flocard, and P.-H. Heenen, Phys. Rev. C **38**, 550 (1988).
- ⁸S. Lunardi, F. Scarlassara, F. Soramel, S. Beghini, M. Morando, and S. Signorini, Z. Phys. A **321**, 177 (1985).
- ⁹C. J. Lister, B. J. Varley, R. Moscrop, W. Gettely, P. J. Nolan, D. J. G. Love, P. J. Bishop, A. Kirwan, D. J. Thornley, L. Ying, R. Wadsworth, J. M. O'Donnell, H. G. Price, and A. H. Nelson, Phys. Rev. Lett. **55**, 810 (1985).
- ¹⁰L. Goettig, W. Gettely, C. J. Lister, R. Moscrop, and B. J. Varley, Nucl. Phys. **A475**, 569 (1987).
- ¹¹F. Soramel, S. Lunardi, S. Beghini, M. Morando, C. Signorini, W. Meczynski, G. Fortuna, G. Montagnoli, and A. M. Stefanini, Phys. Rev. C **38**, 537 (1988).
- ¹²E. S. Paul, K. Ahn, D. B. Fossan, Y. Liang, R. Ma, and N. Xu, Phys. Rev. C **39**, 153 (1989).
- ¹³R. Ma, K. Ahn, Y. Liang, E. S. Paul, N. Xu, and D. B. Fossan, Phys. Rev. C **39**, 530 (1989).
- ¹⁴J. Gilat, J. M. Nitschke, P. A. Wilmarth, K. Vierinen, and R. B. Firestone, in *Nuclei Far from Stability*, Proceedings of the Fifth International Conference on Nuclei Far from Stability, AIP Conf. Proc. No. 164, edited by Ian S. Towner (AIP, New York, 1987), p. 463.
- ¹⁵J. M. Nitschke, P. A. Wilmarth, J. Gilat, P. Möller, and K. S. Toth, in *Nuclei Far from Stability*, Proceedings of the Fifth International Conference on Nuclei Far from Stability, AIP Conf. Proc. No. 164, edited by Ian S. Towner (AIP, New York, 1987), p. 697.
- ¹⁶N. Redon, T. Ollivier, R. Béraud, A. Charvet, R. Duffait, A. Emsallem, J. Honkanen, M. Meyer, J. Genevey, A. Gizon, and N. Idrissi, Z. Phys. A **325**, 127 (1986).
- ¹⁷J. M. Nitschke, P. A. Wilmarth, P. K. Lemmert, W.-D. Zeitz, and J. A. Honkanen, Z. Phys. A **316**, 249 (1984).
- ¹⁸P. A. Wilmarth, J. M. Nitschke, R. B. Firestone, and J. Gilat, Z. Phys. A **325**, 485 (1986).
- ¹⁹J. M. Nitschke, Nucl. Instrum. Methods **206**, 341 (1983).
- ²⁰W. G. Winn, H. H. Gutbrod, and M. Blann, Nucl. Phys. **A188**, 423 (1972); M. Blann and J. Bisplinghoff, computer code ALICE, Livermore, 1982, U.S. Department of Energy (DOE) Report No. UCID-19614, 1982.
- ²¹J. T. Routti and S. G. Prussin, Nucl. Instrum. Methods **72**, 125 (1969).
- ²²R. B. Firestone, J. M. Nitschke, P. A. Wilmarth, and K. Vierinen, Nuclear Science Division 1986-87 Annual Report, Lawrence Berkeley Laboratory Report No. 25295, 1988 (unpublished), p. 46.
- ²³J. B. Cumming, in Proceedings of a Symposium on Applications of Computers to Nuclear and Radiochemistry, Gatlinburg, Tennessee, 1962, edited by G. D. O'Kelly (National Academy of Science Report No. NAS-NS3107, 1963), p. 25.
- ²⁴J. Deslauriers, S. C. Gujrathi, and S. K. Mark, Z. Phys. A **283**, 33 (1977).
- ²⁵R. Turcotte, H. Dautet, S. K. Mark, N. de Takacsy, E. Hagerberg, V. T. Koslowsky, J. C. Hardy, H. Schmeing, and X. J. Sun, in *Nuclei Far from Stability*, Proceedings of the Fifth International Conference on Nuclei Far from Stability, AIP Conf. Proc. No. 164, edited by Ian S. Towner (AIP, New York, 1987), p. 473.
- ²⁶R. Béraud, R. Duffait, A. Emsallem, M. Meyer, N. Redon, D. Rolando-Eugio, D. Barnéoud, J. Blachot, J. Genevey, and A. Gizon, in *Third International Conference on Nuclear Nucleus Collisions, Saint-Malo, France, 1988*, edited by C. Estève, C. Grégoire, D. Guerreau, and B. Tamain (Centre de Publications de l'Université de Caen, Caen CEDEX, France, 1988), p. 3.
- ²⁷P. A. Wilmarth, Ph.D. thesis, University of California, Berkeley, 1988 (Lawrence Berkeley Laboratory Report No. 26101).
- ²⁸*Table of Isotopes*, 7th ed., edited by C. M. Lederer and V. S. Shirley (Wiley, New York, 1978).
- ²⁹M. O. Kortelahti, H. K. Carter, R. A. Braga, R. W. Fink, and B. D. Kern, Z. Phys. A **332**, 229 (1989); K. S. Vierinen, J. M. Nitschke, P. A. Wilmarth, R. B. Firestone, and J. Gilat, Nucl. Phys. **A499**, 1 (1989).
- ³⁰E. S. Paul, R. Ma, C. W. Beausang, D. B. Fossan, W. F. Piel, Jr., S. Shi, N. Xu, and J.-y. Zhang, Phys. Rev. Lett. **61**, 42 (1988).
- ³¹J. Deslauriers, S. Gujrathi, S. K. Mark, and S. P. Sud, Z. Phys. A **325**, 421 (1986).
- ³²P. Möller, private communication; P. Möller and J. R. Nix, Nucl. Phys. **A361**, 117 (1981).